Centrifugal Separation with Emphasis on the Rotational Particle Separator

Erik van Kemenade[1],*, Bert Brouwers[1],[2], Rob van Benthum[1]

Abstract

A review is given of separation methods based on centrifugation. Attention is focused on separation of mixtures of gases and droplets. More particularly we consider: the method of gas centrifuges or ultra-centrifuges to separate gases of different molecular weight, and centrifugal separators to separate droplets from gases. Elementary physical principles are used to formulate basic equations. From here on, rules are derived for separation performance, energy consumption and size of the installations. Status of technology of each of the methods is illustrated by presenting actual cases of application.

Keywords: Centrifuge, Cyclone, Rotational Particle Separator, Vane Separator

Received: June 29, 2014; *revised:* September 22, 2014; *accepted:* September 25, 2014

DOI: 10.1002/cben.201400027

1 Introduction

Removal of unwanted components from gases is one of the common unit operations in process technology [1, 2]. Examples include uranium enrichment, CO_2 removal from flue gases, synthesis gas, and natural gas, scrubbing systems, and dew-point separators [3].

Separation of gases of different molecular weight by ultra-centrifuges is a technology used for the large-scale production of uranium [4]. In [5, 6], the potential of the process is explored for separation of methane and carbon dioxide mixtures. Based on experiments it is concluded that the process is too slow for industrial application. In Sect. 2, it is shown on basic principles that indeed the residence time for this separation method is in the order of hours. For that reason, the primary operation of industrial gas purification processes generally falls in one of the following categories [3]:

- absorbtion into a liquid
- adsorbtion into a solid
- permeation through a membrane
- chemical conversion to another compound
- preferential condensation

All processes that involve a phase change tend to produce very small particles or droplets [7]. Three principles used to achieve physical separation of gas and liquids or solids are momentum, gravity settling, and coalescing. Any separator may employ one or more of these principles, but the fluid phases must be immiscible and have different densities for separation to occur [1].

If the gas is traveling too fast to allow the liquid droplets to settle out under gravity, they become suspended (or entrained) in the gas or vapor. These particles can be separated by fiber bed filters but these are characterized by a very low throughput, leading to large installations [8].

In an inertial separator, a change in flow direction is induced. Separation is now achieved by a combination of centrifugal, gravitational, and inertial forces. A change in flow leads to a pressure drop so the extra energy consumption has to be merited by the reduction in residence time or size. As the residence time in a separator increases with decreasing droplet size, the following order of separation technology with decreasing droplet size is seen in industry [1]:

- gravitational separator
- vane pack
- cyclone

In the rotational particle separator (RPS) under discussion in this paper, the strength of a vane pack separator, that is the small distance to the collecting wall, is combined with the strength of a cyclone, i.e., the high centrifugal force, by introducing a rotating coalescer in a cyclone. In Sect. 3, simple equations for the separation efficiency as function of geometry and flow velocity for vane packs, cyclone, and RPS are derived. In Sect. 4, the flow instabilities that set limitations to separator performance are discussed. In order to validate the separation efficiency equations and to see the onset of instabilities,

[1] Dr. Erik van Kemenade (corresponding author), Prof. Bert Brouwers, Dr. Rob van Benthum
Eindhoven University of Technology, PO box 513, 5600 MB Eindhoven, The Netherlands.
E-Mail: h.p.v.kemenade@tue.nl

[2] Prof. Bert Brouwers
Romico Hold A.V.V., Burg. Cortenstraat 24, 5662 GV Maastricht, The Netherlands.

detailed experiments comparing not only the incoming droplet concentration, but also droplet distribution with the outgoing concentration and distribution are described in Sect. 5. In Sect. 6, the pressure drop of a cyclone is compared to that of a RPS. Both vane-pack and RPS-type separators may need a cleaning system under heavy dry loading. This aspect is discussed in Sect. 7 with the RPS as example.

The design rules of Sect. 2 give a good indication for the separation method to be selected for a given application, detailed experiments and prototyping are necessary to come to a practical design for a given application. In Sect. 8, an example for the development of the RPS as demister in the semi-cryogenic process of condensed rotational separation to remove carbon dioxide from methane is given. Conclusions are presented in Sect. 9.

2 Gas Centrifuges

A gas centrifuge is basically a cylinder, filled with a gas mixture, and rotates at high speed. Due to the large centrifugal forces, the gas is pushed to the wall, resulting in a pressure gradient [9]. Gases with different molecular weights have different partial pressure profiles and their mole fraction profiles vary with radius. The partial pressure of component i is given by [10, 11]:

$$p_i = p_j(0)\exp\left(\frac{M_i\omega^2R^2}{2R_0T}\right) \tag{1}$$

M denotes the molecular weight, ω the angular speed, R the radius, and R_0 the gas constant. For the ratio of the partial pressures of the components, it can be written:

$$\frac{p_i(R)}{p_j(R)} = \frac{p_i(0)}{p_j(0)}\exp\left(\frac{(M_i - M_j)\omega^2R^2}{2R_0T}\right) \tag{2}$$

and the separation factor α that can be achieved is

$$\alpha = \frac{\left(\frac{N}{1-N}\right)_R}{\left(\frac{N}{1-N}\right)_0} = \frac{\frac{p_i(R)}{p_j(R)}}{\frac{p_i(0)}{p_j(0)}} = \exp\left(\frac{(M_i - M_j)\omega^2R^2}{2R_0T}\right) \tag{3}$$

where N is the component concentration. Centrifugal separation technology was developed for separating uranium isotopes introduced into the centrifuge in the form of the gas UF_6 where the aim is to enrich a stream in the lighter isotope from the heavier. The weight difference is only 3 molecular weight units whereas the difference that will be obtained for industrial gas separation is an order larger.

The separation time that is needed is governed by diffusion. A single particle with diameter d_p moving through a gas with a smaller molecular diameter d_1 is considered. d_p is smaller than the mean free molecular path λ. For air under ambient conditions, $\lambda = 0.07\,\mu m$. The mean resistance force experienced by a particle with mean velocity $<u>$ due to collisions is $<F_u> = \beta<u>$. When d_p is much smaller than the mean free length, $\beta = \frac{5}{3}\pi^2\mu d_p^2/\lambda$, where μ denotes the dynamic viscosity [12]. For $d_p >> \lambda$, $\beta = 3\pi\mu d_p$, and combination yields:

$$\beta = \frac{3\pi\mu d_p}{1+C}\ ,\ C = \frac{9\lambda}{5\pi d_p} \tag{4}$$

In a centrifuge, the centrifugal force is $m_p\omega^2<r>$, where m_p is the mass of the particle and equals the resistance force $<F_u>$ so the drift in the Langevin equation can be written as:

$$\frac{\pi}{6}\rho_p d_p^3\omega^2 < r >= \beta\frac{\mathrm{d} < r >}{\mathrm{d}t} \tag{5}$$

or equivalently in the diffusion equation

$$\frac{\mathrm{d} < r >}{\mathrm{d}t} = \frac{\mathcal{D}\Delta M\omega^2 < r >}{R_0T} \tag{6}$$

where D denotes the diffusivity. The time needed for separation can now be estimated as

$$t \approx \frac{R_0T}{\mathcal{D}\Delta M\omega^2} \tag{7}$$

Gas centrifuges typically operate at a speed of $10^3\,rad\,s^{-1}$ [4]. With $D = 10^{-5}\,m^2s^{-1}$, $\Delta M = 25\,g\,mol^{-1}$, and $T = 300\,K$, a typical separation time in the order of hours is obtained. The conclusion is that direct centrifugal gas-gas separation is not practical for large scale industrial separation. Increasing the pressure is not that helpful for component separation in the gas phase, because to a first approximation, the product of diffusion constant and pressure, pD, is constant, that is, at high pressures the diffusion constant decreases.

3 Basic Principles of Inertial Separation

In this section, the principle of inertial separation in three basic geometric configurations is examined: A bend, in which the centrifugal force is induced by forcing the gas to change direction. This is the basis of vane packs (Fig 1 a). In axial cyclones (Fig. 1 b), droplets are centrifuged outwards in the cylindrical (or annular) space downstream of a swirl generator. In a rotating element (Fig. 1 c) the gas is led through channels, rotating parallel to the rotation axis. The distance to the rotation axis is far as compared to the inner (radial) channel height.

3.1 Vane-Type Separators

Vane-type separators are widely used in industry and separate larger (> 10μm) droplets or particles from gases [1]. The vane-type separator is represented by a flow through a single bend (Fig. 2, [13]). Three forces act on a particle moving along a curved trajectory with radius r and velocity v_θ: (i) the centrifugal force F_c, (ii) a drag force F_d, and (iii) a buoyancy force F_{buo}: $F_c = F_d + F_{buo}$. For particles with diameters ranging from about 0.5 μm to 25 μm, the fluid force can be described by Stokes flow [14]. For smaller and larger particles, Cunningham and Reynolds number corrections have to be introduced, respectively, however, at a diameter of 1 μm, the effect is only ca. 10 %.

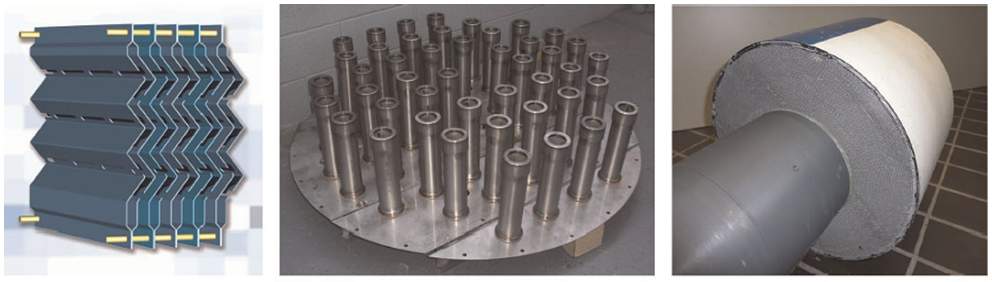

a) Vane pack b) Cyclone deck c) Rotating element

Figure 1. Centrifugal separator configurations.

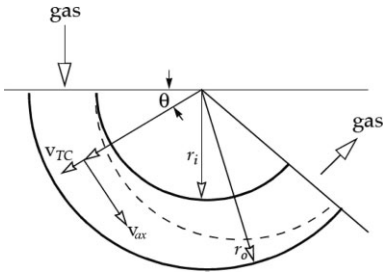

Figure 2. Vane-type separator.

Omitting it is a more conservative approach [15]. The radial migration velocity of a particle can then be described as

$$v_r = \frac{(\rho_p - \rho_f) d_p^2 v_t^2}{18 \mu r} \tag{8}$$

ρ_p and ρ_f are the densities of the particle respectively the carrier fluid. μ denotes the dynamic viscosity of the carrier fluid and v_t the tangential velocity.

The attention can now be focused on the collection efficiency. The trajectory of a particle can be described as $dr/d\theta = rV_r(r)/v_f$ with the assumptions that the velocity is uniform, no secondary flows, and a tangential particle velocity equal to the carrier fluid velocity v_{ax}. Integration gives

$$r(\theta) = r(0) + \frac{(\rho_p - \rho_f) d_p^2 v_{ax}}{18 \mu} \theta \tag{9}$$

With the assumption that the particles are uniformly distributed over the cross section, the efficiency of the separator can be derived as

$$\varepsilon = \frac{r(\theta_{sep}) - r_i}{r_o - r_i} = \frac{|\rho_p - \rho_f| d_p^2 v_{ax}}{18 \mu (r_o - r_i)} \theta_{sep} \tag{10}$$

The particle size that can be separated with 50 % efficiency can now be determined as

$$d_{p50} = \sqrt{\frac{9 \mu d_{ch}}{(\rho_p - \rho_f) v_{ax} \theta_{sep}}} \tag{11}$$

with the channel height $d_{ch} = r_0 - r_i$. With the definition of the particle relaxation time

$$\tau = \frac{d_{p50}^2 (\rho_p - \rho_f)}{18 \mu} \tag{12}$$

Eq. (11) can be rewritten as:

$$\tau_{vane} = \frac{d_{ch}}{\theta_{sep} v_{ax}} \tag{13}$$

In practice, the minimum channel height is restricted to about a millimeter. The velocity is limited by liquid entrainment and droplet break-up. Typical values are below 10 m s^{-1}, so the particle relaxation time that can be achieved with this type of separator is in the order of 10^{-4} s. For air-water under ambient pressure, this corresponds to a minimal d_{p50} value in the order of 10 µm.

3.2 Cyclones

The axial cyclone consists of a stationary cylindrical pipe which contains at the entrance stationary vanes or blades (Fig. 3). Fluid which enters the pipe and passes through these blades attains a swirling motion. Dispersed phase entrained in the fluid acquires this swirling motion as well. Having a density which is higher than the density of the carrier fluid, the dispersed phase will be subjected to a centrifugal force which causes it to move radially toward the cylindrical wall. It leaves the device via outlets situated at the end of the pipe constituting the axial cyclone. To find the d_{p50}, Barth's cyclone model [16] is used with the assumptions that the maximum tangential velocity in the

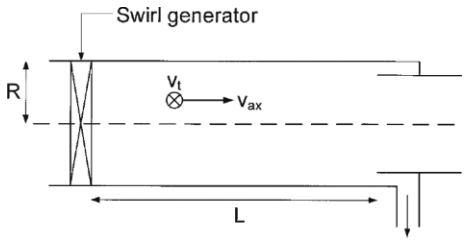

Figure 3. Axial cyclone.

core of the cyclone equals the inlet velocity and slip can be neglected:

$$d_{p50} = \sqrt{\frac{9\mu v_{ax} R^2}{2(\rho_p - \rho_f) v_t^2 L}} \tag{14}$$

v_t is the tangential velocity, L the length of the cyclone, and R the radius. To derive this equation, it is assumed that the axial velocity v_{ax} is constant over the radius.

Typical cyclones have a swirl ratio $S = v_t/v_{ax}$ of 1–2 and a L/R of about 5 [15]. The axial velocity can be higher compared to the vane type: in the order of 20 m s^{-1}. The only free parameter is now the radius: i.e., to achieve a d_{p50} of 10 µm the radius has to be below 0.15 m. For higher volume flows multi-cyclones have to be used.

3.3 Rotational Particle Separator

The inline version of the rotational particle separator (RPS) is an axial cyclone within which a rotating separation element is situated (Fig. 4) [17, 18]. The rotating element consists of a multitude of axially oriented channels of diameter of about 1 to 2 mm. The separation process taking place in the channels of the RPS is similar to that in the cyclone. In this case, for d_{p50} [18] can be derived

$$d_{p50} = \sqrt{\frac{27\mu v_{ax} d_{ch} R}{2(\rho_p - \rho_f) v_t^2 L}} \tag{15}$$

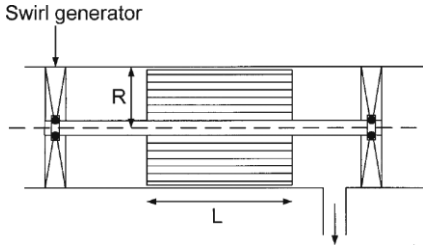

Figure 4. Axial rotational particle separator.

3.4 Comparison of Basic Geometries

Now, the performance of the RPS can be compared to the vane separator by looking at the ratio of d_{p50} for the same axial velocities:

$$\frac{d_{p50,vane}}{d_{p50,RPS}} = \sqrt{\frac{36}{27}\frac{1}{\theta_{sep}}\frac{L}{R}S^2} \tag{16}$$

While the separation angle is limited to about $\theta_{sep} = \pi/2$, the ratio R/L can be used for the RPS to increase performance.

To obtain the same particle relaxation time for the same cyclone parameters v_{ax}, v_t, and R/L, $R = 3d_{ch}$. The d_{p50} for the RPS is constant, while the d_{p50} of the cyclone scales with

$$\frac{d_{p,cyc}}{d_{p,RPS}} = \sqrt{\frac{R}{3d_{ch}}} \tag{17}$$

For equal separation performance the following relation is found

$$\frac{R^2_{cyclone}}{R^2_{RPS}} = \frac{d_{ch}}{3R_{cyclone}} \tag{18}$$

This ratio is a measure for the difference in footprint between the cyclone and RPS for an equal separation performance. For the same separation performance, the footprint of the RPS can be an order lower compared to a cyclone. In the same volume, the RPS can separate particles or droplets that are an order smaller.

Often the performance of a gas demisters is presented in the form of a sizing or load factor as used in the Souders-Brown equation [1]

$$V_t = K\sqrt{\frac{\rho_p - \rho_f}{\rho_f}} \tag{19}$$

The load factor or characteristic gas velocity K is a direct measure for the required footprint of the installation and has the unit of velocity. In Fig. 5, the K value for the RPS is compared to state of the art demisters.

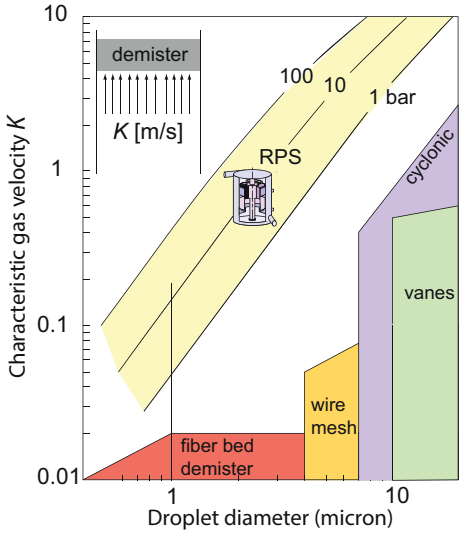

Figure 5. Load or sizing factor of demisters. Adapted from [5].

3.5 Closure

Based on, among other things, the simplifying assumption of uniform axial flow, a general expression for inertial separation efficiency is derived as a function of dimensionless droplet size. In [19, 20], their influence was investigated on the velocity profile and channel shape. The influence of the Rankine vortex on the separation performance is studied in [15, 21]. These effects turn out to be of second order to the separation performance.

Flow instabilities and turbulence however may destroy separation performance and are discussed in the next section.

4 Flow Instabilities

Although at first glance simple and straightforward, the radial motion of phases and particles in a channel is a subtle and sensitive process. The smallest fractions aimed of being separated are those which move with a radial velocity which compares to the axial fluid velocity as the ratio of channel height to channel length: cf. Eq. (15). In practical applications of the rotational particle separator this ratio is very small, typically < 0.01. So the smallest separated fractions move with radialvelocities which are only one percent of the axial fluid velocity. If now secondary fluid flows occur in planes perpendicular to the axial channel axis which are only one percent in magnitude of the axial fluid velocity, the process of radial migration of the smallest separated fraction may already be disturbed.

Unwanted secondary flows can occur in case the symmetry axis of a channel is at an angle with respect to the rotation axis: For example, by fabrication inaccuracy, the channels can be twisted around the symmetry axis of the filter element, or they can diverge or converge as their distance from the axis of the filter element increases (or decreases) in axial direction. Coriolis forces will act on the fluid as soon as the fluid flow is nonparallel to the rotation axis. Such forces lead to circulatory secondary flows in planes, perpendicular to the axial channel axis [23] of a kind similar to the circulatory flows in bends. For circular pipes, it is possible to calculate these flows analytically as solutions of the Navier-Stokes equation obtained under certain limiting conditions which coincide with the conditions under which the rotational particle separator operates [24]. In practical design it implies that nonparallelity of channels must be limited to specific values, to angles of inclination of a few degrees in typical cases.

Usually, the flow in the channels of the filter element is kept in the laminar regime to prevent capture of particles or droplets in turbulent eddies or swirls. In case of large volume and or high pressure applications, the laminar flow condition may impose a too severe restriction on the design.

In most cases, the Reynolds number is low enough for the flow and particle behavior to be studied in detail by means of direct numerical simulation (DNS) of the fluid flow and Lagrangian particle tracking [25]. The results of DNS reveal that an axial vortex is present in the flow, caused by the rotation, but also that this vortex hardly influences the collection efficiency. However, turbulent velocity fluctuations have a negative influence on the collection efficiency, especially for larger particles (Fig. 6). In order to meet design criteria in practice, the length of the RPS should be chosen about 20 % larger than laminar design criteria prescribe to obtain the same collection efficiency. The results confirm that when the rotational particle separator is used as a bulk separator and a strictly defined cut-off diameter is not required, the working range can be extended in the turbulent range to enhance the throughput within the same volume constraints. This is a major advantage in offshore applications where platform space and load capacity are at premium and in recent designs of the RPS for natural gas treatment that operate in the turbulent regime [20, 26].

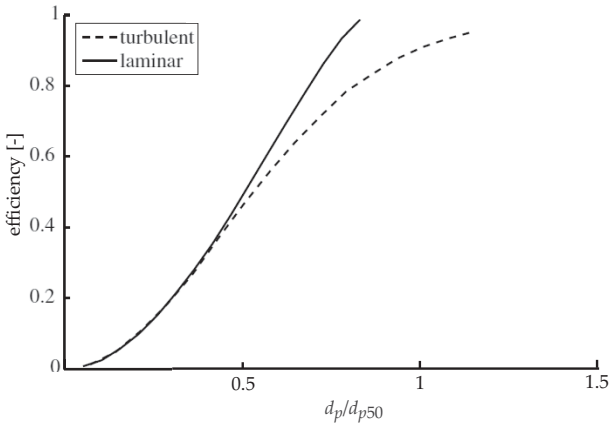

Figure 6. Efficiency of the RPS for laminar and turbulent flow [18].

5 Experiments

Two measurement methods are used to assess the performance of centrifugal separators: laser diffraction and impactation. Laser diffraction is based on the phenomenon that particles illuminated by a laser beam scatter light at angles that are inversely proportional to the size of the particles. Large particles scatter at small forward angles while small particles scatter light at wider angles. Mie theory is used to establish the relation between the scattered energy distribution on the detectors and the particle size distribution. In both cases, the measurement setup is such that the droplet distribution of a nozzle can be measured with and without the separator in place. If the nozzle droplet distribution overlaps the separator cut-off diameter, the separator efficiency as function of the size can be deduced from both droplet size distributions. The other apparatus used is an Anderson-type cascade impactor whereby particles within a size class are collected on a specific stage of the impactor.

5.1 Vane-Type Separator

As representative for bend-type separators, a moisture separation panel as applied to the inlet of turbo machinery was used. The experimental set-up was similar to [27] and comprises a Malvern Mastersizer S laser diffraction device. Based on the fixed dimensions of the laser diffraction device, a square test duct with external dimensions of 220 mm was used to guide the air and droplets to the water droplet panels and through the Mastersizer (Fig. 7). Complying with standard installation, a fan was installed downstream of the duct. The laser measurement is located about 300 mm downstream of the outlet of the water droplet catcher panels to have sufficient mixing downstream the separator panel without significant evaporation of the droplets. Before each spray spectrum measurement is done, with or without the moisture separator panel in place, the set-

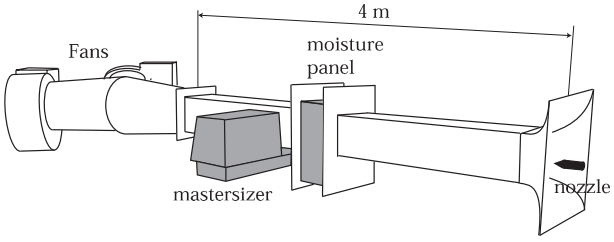

Figure 7. Experimental set-up.

ting of the fan is checked by measuring the velocity in the middle of the duct with a hot wire measuring device. Analysis of the moisture separator panels was done at 3 m s^{-1} and 5 m s^{-1}.

A typical measurement result is depicted in Fig. 8. Each data point represents three measurements of both the nozzle distribution and the distribution after the separator. Curve (1) is the measured droplet volume distribution without a separator in the duct. Curve (2) is measured with the separator mounted between the nozzle and the measuring spot. Curve (3) is curve (2) scaled to curve (1) using the measured concentration. The probability P that a particle of a certain diameter passes through the separator is found by dividing the values of curve (3) by those of curve (2). The efficiency is equal to the probability that a particle is caught in the separator or $\varepsilon = 1 - P$. Conventionally the cut-off diameter of a separator is characterized by the d_{p50}; the diameter of the particle that has a 50 % probability of passing through the separator (22 µm in the case of Fig. 8). The reached accuracy is below 5 % in the efficiency.

The measured efficiencies scaled to their respective d_{p50} are presented in Fig. 9. The three panel types have slightly different geometries but all panels essentially depend on two bends for the removal of droplets. Consequently, the curves overlap each other despite their difference in d_{p50}. The exception is panel type 3 at the higher velocity of 5 m s^{-1}, here re-entrainment or flooding occurs, a phenomenon reported since 1939 [28]. It can be concluded that the d_{p50} indeed is a good measure to compare the performance of geometrically similar moisture

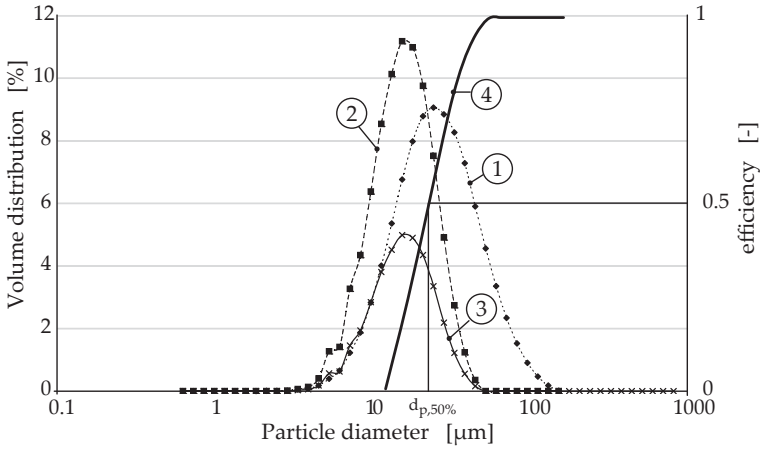

Figure 8. Typical measurement result: Curves (1) to (2) are the volume distributions measured without and with separator present. Curve (3) is curve (2) scaled to (1). The efficiency curve (4) is obtained as 1–(3)/(1).

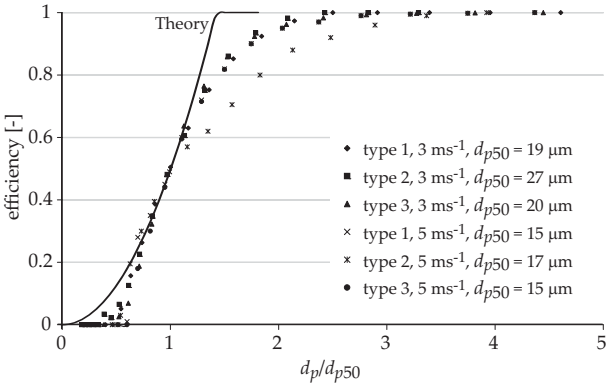

Figure 9. Measured panel efficiency.

panels as the efficiency distribution hardly changes. Nevertheless, the distribution should be measured to establish the operating limits of a specific panel.

5.2 Cyclone

The demisting stage of gas-liquid scrubber vessels usually consists of a bank of axial cyclones (swirl tubes), working in parallel. The efficiency of a single commercial swirl tube was measured in the way explained in the previous section. Since the droplets leaving the cyclone are in the range 1–10 µm, the lens of Malvern's Mastersizer S was too small; instead the Spraytec was used.

During measurements the cyclone was contained in a bigger pipe (diameter 200 mm), simulating a scrubber vessel with upwards gas flow. Nozzles injected a constant amount of water into an adjustable airflow. Droplet distributions and concentrations were measured in the open outflow above this pipe. The efficiency is determined taking a dummy cyclone without swirl element, i.e., vanes and body removed, as reference. Measurements were done at eleven flowrates, for which the corresponding values of d_{p50} were calculated according to Eq. (14). Fig. 10 shows the combined result of all measured efficiency curves [21].

5.3 Rotational Particle Separator

Many RPS devices have been designed and tested over the past 15 years, e.g., ash removal from flue gas of combustion installations, air cleaning in domestic appliances, product recovery in pharmaceutical and food industry, oil/water separation and gas demisting, see Fig. 11 [17, 19, 20, 26, 29, 31, 32]. Particle collection efficiencies were determined by measuring distributions at the inlet and outlet using cascade impactors and laser particle counter techniques. For each of the cases, the value of d_{p50} was calculated according to Eq. (15). These were subsequently used to generate separation efficiency distributions as a function of dimensionless particle diameter d_{p50}. Results are shown in Fig. 12. For rea-

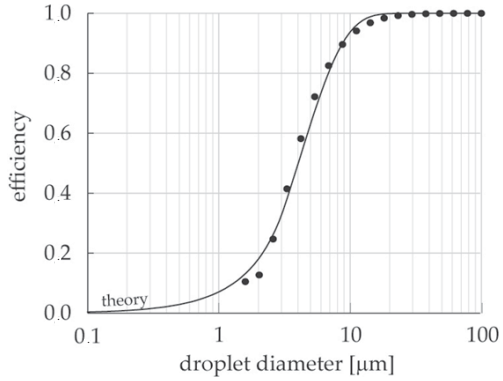

Figure 10. Measured cyclone efficiency as a function of the particle size.

sons of comparison, the theoretical curve is shown as well. The results of the measurements are consistent with each other and compare sufficiently well with theory for design purposes.

5.4 Closure

The basic equations of Sect. 3 describe the performance of well-designed centrifugal separators well in the absence of flow instabilities mentioned in Sect. 4 and can be used for a first order comparison of performance. For the design of these devices a detailed numerical and experimental analysis of the flow is however still required to find the real performance, see [15, 27] amongst others.

6 Power Consumption

The power consumption of both RPS and cyclone is investigated in detail in [15]. Energy consumption occurs mainly through the pressure drop the fluid undergoes when flowing through the apparatus. One can assume that swirl induced at the entrance, and associated radial pressure buildup, is eventually lost: the irreversible pressure loss can be taken equal to $\rho_f v_t^2$. The total work loss can be calculated by integrating over all radial positions. For v_t and v_{ax} constant with respect to r, the result is $\dot{E} = \rho_f v_t^2 Q$, where Q is the volume flow. Energy consumption per unit mass flow $e = \dot{E}/(\rho_f Q)$ then amounts to $e = v_t^2$.

Figure 11. Rotational particle separator designs.

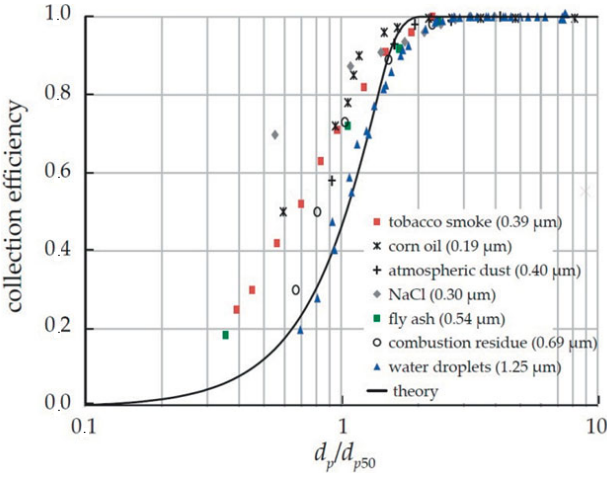

Figure 12. Efficiency of the rotating particle separator.

The flow through the channels of the filter element of the RPS constitutes an extra pressure loss of $\Delta p_{ch} = \rho_f v_{ax}{}^2 f L/(2d_{ch})$. The friction factor for laminar flow in a round channel is $f = 64\mu/(\rho v_{ax} d_{ch})$. Here, the extra pressure losses due to entrance effects, as well as blockage of channels, are disregarded in practice these amount to < 10 % of the channel pressure drop. It has been shown that as liquid builds up on the channel walls, shear stress exerted on the liquid is large enough to tear the liquid stream into large separable droplets downstream of the rotational particle separator [28]. For the specific energy consumption, the following can be written:

$$e_{ch} = \frac{S64\mu L}{\rho_f d_{ch}^2} v_t = O(1) v_t \tag{20}$$

which, in most cases, can be neglected compared to the swirl term v_t^2. It can therefore, be concluded that the energy consumption of an RPS is comparable to a cyclone in first order.

7 Loading

For certain applications, filter cleaning involves removal of the filter element from the apparatus and followed by cleaning and reintroduction or by replacement. For most industrial applications, however, in situ filter cleaning is preferred, with or without limited interruption of the filtering process.

For air-jet cleaning, a nozzle is fitted on top of the rotational particle separator which can move radially from inner to outer radius of the filter element. Once the channels of the filter element become saturated with particulate material, the jet starts to blow into the channels. This can occur during normal filter operation. The radial width of the noz-

zle compares in size with the height of the channels, i.e., a few millimeters. Due to filter rotation, a moment will occur when the channel has passed the column of air blown from the nozzle. At this moment, expansion waves start to develop from the top of the channel resulting in intense cleaning of the channels [22]. It has been established that about 1 kg of fine particles material collected in the channels can be removed by injecting about 1 kg of compressed air at 6 bar.

As alternative to air or other gases, cleaning of the filter element may be accomplished by periodically injecting water or other liquids. In practice, it has been established that (hot) water at pressures of 50 to 100 bar can be injected using the same nozzle as the one used for air. It offers the possibility to clean the filter from time to time very thoroughly with (hot) water, in addition to a regular air cleaning. It is particularly interesting for applications where high standards of hygiene apply.

A third method for removing particle material from the channels of the filter element is to continuously add liquid. This can occur by dispersing a spray of fine liquid particles which are subsequently centrifuged towards the outer walls of the channels of the filter element. Here, they form a liquid film which moves downwards and which carries away the other (solid) particles. The wet version of the rotational particle separator appears to be an attractive alternative to existing wet scrubbers often employed in the chemical and process industry. In contrast to wet scrubbers, in the rotational particle separator water is not injected to separate particles, but only to transport particle material being centrifuged towards the walls. This results in much lower, by up to two orders of magnitude, amounts of washing liquids [32].

In liquid applications, a film is builds up along the walls of the channels. The speed at which the film can be drained determines the maximum liquid load. Both theory and experiments show that liquid loads up to 50 $\%_{mass}$ can be drained effectively [33, 34].

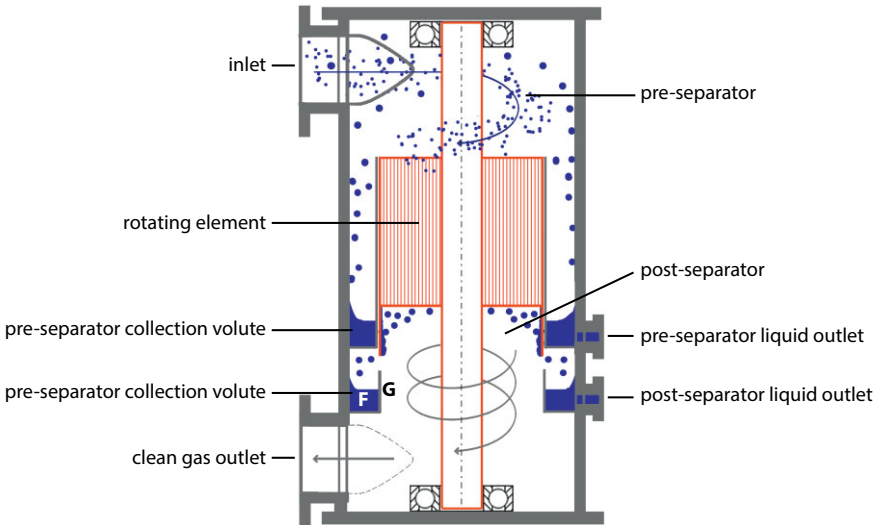

Figure 13. High volume RPS demister design.

8 Rotational Particle Separator Demister

The introduction of the RPS as a gas demister in large volume applications [32] presented a number of new design issues, the most important being the behavior under high pressure and the ability to cope with large liquid loads. In this section, the development of the RPS demister is described.

8.1 Rotational Particle Separator Demister Design

Gas containing a mist of droplets enters the unit via a tangential inlet (Fig. 13). First coarse droplets, larger than 10 µm, are separated in the pre-separator section. The pre-separator acts as a cyclone and collects the droplets in the stationary pre-separator collection volute. This liquid leaves via the tangentially connected pre-separator liquid outlet.

The gas stream, containing the remaining mist of mainly micron-sized droplets, enters the rotating element (Figs. 13 and 14 a). In the design point the rotating element can be driven by the impulse of the rotating flow. An external drive and freewheel can be added for rotating speed, and thus separation, control. While traveling in the axial direction through the rotating channels, the droplets are driven to the channel walls by centrifugal force and coagulate into a thin film (Fig. 14 b). The rotating element thus acts as a droplet coalescer. For optimal film behavior and minimal pressure drop the flow direction through the element is downward [17] out of the channels. Due to gravitational and shear forces, the film is forced.

At the end of the channels the film breaks up into droplets of typically 50 µm (Fig. 14c). The outer wall of the rotating element extends in the axial direction beyond the end of the channels the post-separator section (Fig. 13). This ensures that the solid body rotation of the gas stream leaving the element is maintained. Droplets that break up at the end of the channels are centrifugally separated from the gas in this rotating field, and collected in a film on the rotating outer wall.

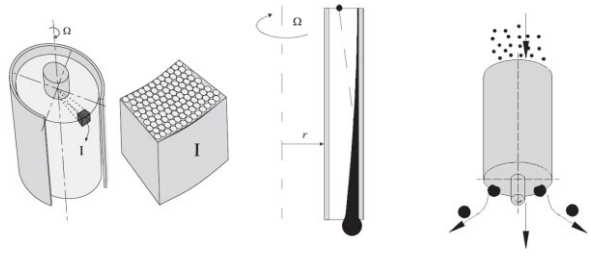

a) rotational element and closeup b) film formation c) droplet break-up

Figure 14. Principle of a rotating element.

The liquid film leaves the gas stream at the end of the extended outer wall of the rotating element towards a non-rotating post-separator collection volute. The liquid still contains significant momentum, which drives a standing film (*F*) within the stationary volute. Via the tangentially connected post-separator liquid outlet, the liquid leaves towards a collection vessel. The inner wall of the collection volute (*G*) keeps the liquid separated from the product gas flow. This wall prevents re-entrainment of liquid due to splashing in the post-separator.

8.2 Prototypes

The capability of the RPS to separate micron sized droplets is also the core of the process of condensed rotational separation whereby a phase change is induced to separate unwanted components from gases. In CRS, droplet wise partial condensation is induced by fast pressure and temperature reduction (expansion in a Joule-Thomson valve or a turbo-expander. Fast expansion generates instant bulk-cooling, which supersaturates the gas when expanded into a vapor-liquid two-phase region and drives condensation by means of nucleation and droplet growth. Within milliseconds, a mixture of vapor and micron sized droplets is obtained in concentrations according to thermodynamic phase equilibrium [36].

The first prototype (Fig. 15 a) was a bench scale unit designed for low temperature separation of CO_2 from CH_4 and N_2 in a lab scale expansion pilot (–55 °C, 27 bar, 60 $nm^3 h^{-1}$) to verify the CRS principles [17, 37, 38].

Since centrifugal separation is a process that is sensitive to design details that are easily overlooked in CFD simulations, a visually accessible industrial scale prototype (natural gas flow equivalent 90 000 $nm^3 h^{-1}$ at 40 bar, –55 °C) has been built. This RPS was operated with water and air under ambient conditions (Fig. 15 b) to investigate subsequently high liquid loading and separation performance under semi-turbulent conditions in the rotating element [17, 21]. Performance was found to be according to expectations.

The next step was a pressurized RPS-demister, capable of handling a flow of 920 $nm^3 h^{-1}$ at 8 bar and –20 °C, to proof construction according to industrial standards [20]. This RPS was tested at Eindhoven University with water and air in the same way the atmospheric 90 000 $nm^3 h^{-1}$ prototype was tested. Again, the performance was found to be in agreement with design specifications [20]. In 2013, this RPS was subsequently installed in a slipstream of Enexis' gas grid (Fig. 15 c) behind a pressure reduction section (40 to 8 bar) for the removal of heavy liquid contaminants and is running since summer 2013. In phase II of the Enexis project this RPS demister shall be replaced by an up-scaled version that takes on the full natural gas flow of 6500 $nm^3 h^{-1}$.

9 Conclusions

It has been shown that a purely gaseous separation process is too slow for practical application. Process intensification can be achieved by condensation of molecules to much larger particles. The separation performance of centrifugal separators expressed as the diameter of the particle that has 50 % chance of separation, d_{p50}, is a function of three independent process parameters: residence time, specific energy consumption, and volume flow. These three parameters can be used as a basis for comparison between different separator configurations.

If the carrier fluid is a gas, then the separation performance of a centrifugal separator as a function of volume flow varies only slightly with pressure. An increase in operating pressure leads at equal mass flow rate to a smaller volume flow rate, and thus, to a better separation performance or smaller equipment.

The RPS can catch droplets down to 1 µm with practically 100 % efficiency. The principal advantage of the RPS over the cyclone thus is that for same residence time, i.e., building volume, and same rotational speed, i.e., pressure drop, it can separate much smaller droplets, typically 5 to 10 times smaller. Alternatively the RPS can separate the same droplet size as a cyclone in a 10-times smaller volume. The pressure loss amounts to roughly 2 % of the pressure of the incoming gas.

To proof reliability, a RPS is designed, manufactured and installed in a natural gas distribution station to remove condensate. A new RPS for the full flow of 6500 $nm^3 h^{-1}$ is ready for installation. Low temperature separation offers a large energy advantage compared to absorption techniques.

The authors have declared no conflict of interests.

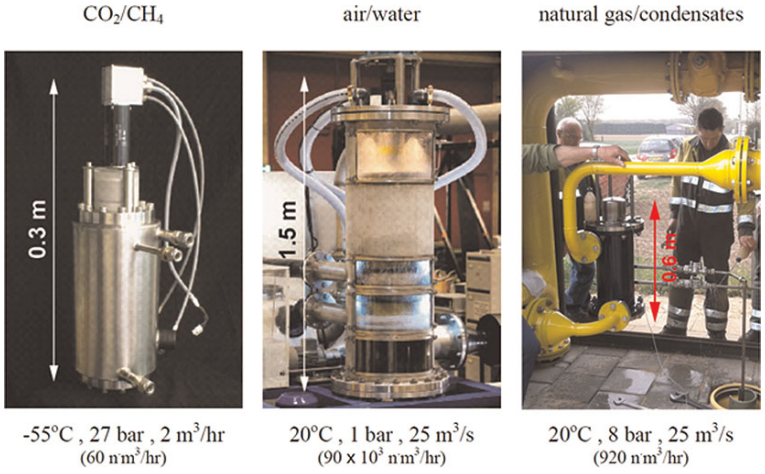

Figure 15. Constructed RPS-Demisters.

H. P. (Erik) van Kemenade is a mechanical engineer (M.Sc. 1989, Ph.D. 1995) with a special interest in the design of innovative heat and mass transfer equipment and processes. After working at Level Energy Technology b.v., he returned to Eindhoven Technical University (TU/e) in 1999. He works with Bert Brouwers on the development of the rotational particle separator for the oil and gas industry, condensing heat exchangers for emission reduction in biomass systems and gas separation processes, and process development and equipment sizing for condensed rotational separation. Dr. ir van Kemenade teaches courses in high temperature constructions, process equipment, innovative process design, and energy conversion.

J. J. H. (Bert) Brouwers is a mechanical engineer (M.Sc. 1972, Ph.D. 1976) and founder of the Romico companies. In 1972, he joined the Ultra Centrifuge Laboratory of UCN/Urenco in Amsterdam and became the Head of Isotopes Separations Research in 1974. In 1979, he joined Royal/Dutch Shell, first as the Group Leader in Offshore Research before moving to London in 1983 to become Staff Member Economics. He was appointed Full Professor of Thermal Engineering at Twente University (1986) before returning to TU/e in 1998 to chair the Process Technology Section of the Mechanical Engineering Department. Prof. Brouwers devised the Rotational particle separator and related processes of condensed rotational separation. IP rights are vested in Romico Hold A.V.V. of which he is CEO.

Symbols used

C	[–]	factor
D	[$m^2 s^{-1}$]	diffusion constant
$\dot{E}$	[W]	work loss
d	[m]	diameter
e	[$m^2 s^{-2}$]	specific power per unit mass flow
F	[N]	force
f	[–]	friction factor
K	[$m\,s^{-1}$]	load factor
M	[$g\,mol^{-1}$]	molecular mass
p	[bar]	partial pressure
Q	[$m^3 s^{-1}$]	volume flow
R	[m]	radius
r	[m]	radius
R_0	[$J\,K^{-1} mol^{-1}$]	universal gas constant
S	[–]	swirl ratio
T	[K]	temperature
t	[s]	time
u	[$m\,s^{-1}$]	velocity
V	[$m\,s^{-1}$]	velocity
v	[$m\,s^{-1}$]	velocity

Greek symbols

α	[–]	separation factor
β	[$Ns\,m^{-1}$]	factor
ε	[–]	efficiency
λ	[m]	free molecular path
μ	[Pa s]	dynamic viscosity
ρ	[$kg\,m^{-3}$]	density
t	[s]	time constant
θ	[rad]	angle
ω	[$rad\,s^{-1}$]	angular velocity

Subscripts

ax	axial
buo	buoyancy
c	centrifugal
ch	channel
d	drag
f	fluid
p	particle
r	radial
t	tangential

References

[1] *GPSA Engineering Data Book*, Gas Processors Suppliers Association, Tulsa, OK **2012**.
[2] *CRC Handbook of Chemistry and Physics*, 89th ed., CRC Press, Boca Raton, FL **2008**.
[3] A. Kohl, R. Nielsen, *Gas Purification*, Gulf Publications, Houston, TX **1997**.
[4] J. F. A. Delbeke, G. Eklund, B. P. M. Van Esch, G. Janssens-Maenhout, W. Janssens, *Energy* **2010**, *35 (8)*, 3123–3130. DOI: 10.1016/j.energy.2010.02.039
[5] M. Golombok, K. Bil, *Ind. Eng. Chem. Res.* **2005**, *60 (16)*, 4397–4407.
[6] R. J. E. van Wissen, M. Golombok, J. J. H. Brouwers, *Chem. Eng. Sci.* **2005**, *53*, 374–380.
[7] W. C. Hinds, *Aerosol Technology*, John Wiley and Sons, New York **1982**.
[8] *Gas/Liquid Separation Technology*, Sulzer Chemtech, Winterthur **2012**, http://www.sulzer.com/en/-/media/Documents/ProductsAndServices/Separation_Technology/Mist_Eliminators/Brochures/Gas_Liquid_Separation_Technology.pdf (accessed June 26, 2014).
[9] J. J. H. Brouwers, *Nucl. Technol.* **1978**, *39*, 311–322.
[10] F. Aston, E. Lindemann, *Phil. Mag.* **1919**, *6 (37)*, 523.

[11] K. P. Cohen, *The Theory of Isotope Separation as Applied to the Large-Scale Production of U-235*, McGraw-Hill, New York **1951**.
[12] N. A. Fuchs, *The Mechanics of Aerosols*, Dover Publications, New York **1964**.
[13] J. J. H. Brouwers, H. P. van Kemenade, J. P. Kroes, *Filtration* **2012**, *12*, 49–60.
[14] R. B. Bird, W. E. Stewart, E. N. Lightfoot, *Transport Phenomena*, John Wiley and Sons, Hoboken, NJ **2007**.
[15] R. J. E. van Wissen, J. J. H. Brouwers, M. Golombok, *AIChE J.* **2007**, *53*, 374–380. DOI: 10.1002/aic.11074
[16] W. Barth, *Brennst. Waerme Kraft* **1956**, *8*, 640–643.
[17] G. P. Willems, *Ph.D. Thesis*, Eindhoven University of Technology **2009**. http://alexandria.tue.nl/extra2/200911885.pdf
[18] A. C. Hoffmann, L. E. Stein, *Gas Cyclones and Swirl Tubes: Principles, Design And Operation*, Springer, Berlin **2008**.
[19] E. van Kemenade, E. Mondt, T. Hendriks, P. Verbeek, *Chem. Eng. Technol.* **2003**, *26 (11)*, 1176–1183. DOI: 10.1002/ceat.200301803
[20] R. Buruma, B. Brouwers, E. van Kemenade, *Chem. Eng. Technol.* **2012**, *35 (9)*, 1576–1582. DOI: 10.1002/ceat.201200188
[21] J. P. Kroes, *Ph.D. Thesis*, Eindhoven University of Technology **2012**. http://purl.tue.nl/706335649322755
[22] J. J. H. Brouwers, *Exp. Therm. Fluid Sci.* **2002**, *26 (2–4)*, 325–334. DOI: 10.1016/S0894-1777(02)00144-9
[23] J. J. H. Brouwers, *Appl. Sc. Res.* **1995**, *55 (2)*, 95–105. DOI: 10.1007/BF00868465
[24] B. P. M. Van Esch, J. G. M. Kuerten, *J. Turb.,* **2008**, *9 (4)*, 1–17. DOI: 10.1080/14685240701847837
[25] J. G. M. Kuerten, B. P. M. van Esch, H. P. van Kemenade, J. J. H. Brouwers, *Int. J. Heat Fluid Flow* **2007**, *28 (4)*, 630–637. DOI: 10.1016/j.ijheatfluidflow.2007.03.003
[26] E. Mondt, E. van Kemenade, R. Schook, *Chem. Eng. Technol.* **2006**, *29 (3)*, 375–383. DOI: 10.1002/ceat.200500395
[27] E. Brunazzi, A. Paglianti, A. Talamelli, *AIChE J.* **2003**, *49 (1)*, 41–51. DOI: 10.1002/aic.690490106
[28] H. Houghton, W. Radford, *T. Am. Chem. Eng.* **1939**, *35*, 427–433.
[29] J. J. H. Brouwers, *Chem. Eng. Technol.* **1996**, *19 (1)*, 1–10. DOI: 10.1002/ceat.270190102
[30] S. Jacobsson, T. Austrheim, A. C. Hoffmann, *Ind. Eng. Chem. Res.* **2006**, *45 (19)*, 6525–6530. DOI: 10.1021/ie051200s
[31] G. P. Willems, J. P. Kroes, M. Golombok, B. P. M. van Esch, H. P. van Kemenade, J. J. H. Brouwers, *J. Fluids Eng.* **2010**, *132 (3)*, 031301. DOI: 10.1115/1.4001008
[32] E. Mondt, H. P. van Kemenade, J. J. H. Brouwers, E. A. Bramer, *Proc. of the 3rd Int. Symp. on Two Phase Flow Modelling and Experimentation*, (Eds: G. P. Celata, P. Di Marco, A. Mariani, R. K. Shah) Edizioni ETS, Pisa **2004**, 1845.
[33] E. Mondt, B. Brouwers, E. van Kemenade, *Chem. Eng. Technol.* **2007**, *30 (5)*, 593–600. DOI: 10.1002/ceat.200700005
[34] G. P. Willems, B. P. M. van Esch, J. J. H. Brouwers, M. Golombok, *Chem. Eng. Sci.* **2008**, *63 (13)*, 3358–3365. DOI: 10.1016/j.ces.2008.04.009
[35] E. Mondt, *Ph.D. Thesis*, Eindhoven University of Technology **2005**. http://alexandria.tue.nl/extra2/200513466.pdf
[36] R. J. van Benthum, *Ph.D. Thesis*, Eindhoven University of Technology **2014**. http://repository.tue.nl/762323
[37] G. P. Willems, M. Golombok, G. Tesselaar, J. J. H. Brouwers, *AIChE J.* **2010**, *56 (1)*, 150–159.
[38] G. D. Bansal, M. Golombok, J. J. H. Brouwers, *Ind. Eng. Chem. Res.* **2011**, *50 (5)*, 3011–3020.

